International Journal of Engineering and Technology Innovation, vol. 4, no. 1, 2014, pp. 01-17

Micro-Satellite Configuration of Discoid and Asymmetrical, Gyroless with Thrusters Three-Axis Robust Control and Stability Analysis

Ho-Nien Shou*

Department of Aviation & Communication Electronics, Air Force Institute of Technology, Kaohsiung, Taiwan, R.O.C.

Received 11 June 2013; received in revised form 05 October 2013; accepted 28 November 2013

Abstract

The center of mass of the micro-satellite can offset due to fuel consumption in the course of propulsion, with the interference of external orbital environment such as gravity gradient torque and solar radiation torque. If the structural shape is discoid and asymmetrical, the attitude control may be difficult. The only solution is to design a robust controller, so that the attitude pointing of the satellite can meet the mission requirements with the interference of internal parameter perturbation and external disturbance. Meanwhile, in order to reduce the weight and manufacturing cost of satellite, in the design of satellite attitude angular rate determination, the project used unscented kalman filter (UKF) algorithm, coarse sun sensor (CSS) and earth horizon sensor (EHS) as measurement components to obtain the satellite attitude without rate gyro.

Keywords: H_∞ controller, unscented kalman filter, coarse sun sensor, earth horizon sensor.

1. Introduction

The stability analysis of discoid and asymmetrical satellite propulsion mode attitude control with large mass change in the paper developed a real-time dynamic simulation system based on the experience in previous studies and the technology developed from annual plan. The attitude control processor was used to test the processor-in-the-loop, in order to be used in the micro-satellite system. The establishment of this analytic method and control technique is very important for controlling the micro-satellite attitude stabilization in any shape with large mass change.

The basic attitude sensors of satellite include attitude sensors and attitude rate sensors. The attitude sensors include sun sensor, horizon sensor, magnetometer, and star tracker. The attitude rate sensor is only the gyro which is very expensive and unreliable in terms of reference point drift and main measurement error source and it is likely to be faultier than attitude sensors. As the satellite technology is generalized, the satellite price needs to reduce. In addition, as the software and algorithmic techniques develop, processing the attitude data by software to obtain attitude rate information becomes mature; thus, the gyro is certainly the first component that engineers aim to remove and the gyro-less design is the research trend in recent years.

(1) The gyroless satellite attitude determination algorithm provided by the UKF is used in this study. The filtering algorithm does not need to carry out linear approximation of the measure equation, while it can improve the attitude determination performance of satellite at large attitude angles effectively. The algorithm has higher convergence as the robust tracking is adopted. The simulation result shows that the algorithm can increase the attitude estimation convergence rate of gyroless satellite in initial attitude tumbling and three-axis stabilization effectively, and also can implement attitude

* Corresponding author. E-mail address: longlifeshow@xuite.net
Tel.: +886-7-625-8738; Fax: +886-7-625-6530

tracking in high speed rotation. The algorithm has concise linear structure. The computing load meets real-time requirement. The structure is simple, and the requirement for hardware configuration is not strict. It is especially applicable to low-cost micro-satellites.

(2) The satellite attitude control has robust performance design issue with internal parameter perturbation and external disturbance. The mass center of satellite offsets due to fuel consumption in the course of propulsion, causing internal parametric variation. If the configuration is asymmetrical, the attitude control may be difficult. The micro-satellite is disturbed by external disturbances of gravity gradient torque and solar radiation torque in orbital motion. A robust controller is thus designed to render the attitude pointing meet the mission requirement.

(3) The geomagnetic environment in the near-earth space is an important resource available for satellites. The magnetometer implements attitude computation by observing the geomagnetic field intensity vector. It is the attitude determination means commonly used by low orbit micro-satellites. The magnetometer is fixed in three-axis direction of the body coordinate system, and can detect the size and orientation of magnetic field at the same time. Moreover, it can compute the attitude after comparison with the magnetometer on the satellite. The measurement of earth orientation vector is implemented by the earth horizon sensor. This measuring method uses the infrared radiation of earth to measure the orientation of the satellite in relation to local horizon. At present, the technique implemented in Formosat-3 is static wide field of view (FOV). The earth sensor can obtain the nadir orientation, the FOV of sensor is required strictly for low-orbiting satellites, and the implementation cost shall be low. The sun azimuth vector is the third available reference vector. The sun sensor measures the orientation of sun sight in sensitive coordinate system according to the solar radiation intensity difference when the attitude changes. This method is the most extensively used attitude determination method. The sun can be approximately regarded as a point source with high intensity, and varying with time. These characteristics guarantee the simple sensing principle, easy design and production, light structure and conveniently implemented attitude determination. The coarse sun sensor (CSS) for sun vector, or called sun sensor implements omnidirectional viewing, but the sun sensor is unavailable in earth's shadow area. The sun sensor, EHS and magnetometer are used in this study as direct observation equation.

(4) The measurement often has errors. The attitude filtering algorithm can reduce the effect of measurement errors on the entire control loop to increase the accuracy. In some states, some sensors fail or the measurement accuracy declines severely, the attitude information cannot be obtained completely, and the single-point deterministic attitude computation is no longer tenable. The filtering processing is required to be imported into the attitude determination loop to enhance the robustness of the system. This study used unscented Kalman filter algorithm to implement six-dimensional attitude estimation output of two/three observation vectors without angular rate sensor. The numerical simulation showed that its performance meets the requirement.

The quaternion is used to describe satellite attitude. The H_∞ controller is used to meet the mission requirement, and UKF algorithm is used to reduce the estimation bias of angular rate. The gyroless performance of micro-satellite is improved effectively in the case of small increase in the amount of calculation. The initial convergence of the algorithm is accelerated, and the ability to control rapid attitude motion is obtained.

The remainder of this paper is organized as follows: Section 2 describes the satellite attitude; Section 3 presents the micro-satellite attitude control model; Section 4 introduces the unscented kalman filtering and algorithm; Section 5 describes the measurement reference model; Nonlinear H_∞ robust control law derived in the Section 6; Section 7 analyzes the attitude determination subsystem; and Section 8 offers the conclusion.

2. Satellite Attitude Description

2.1. Coordinate system and orbit parameters

The coordinates system is defined in order to describe the attitude motion of satellite. The coordinate systems and orbit parameters used in this paper are defined as follows:

(1) The origin of geographic coordinate is the location point of satellite on the earth surface (or subpoint on earth surface); x axis points to the east, y axis points to the north; z axis points to the earth center in local vertical direction; x axis, y axis and z axis form a right-handed coordinate system, i.e. so-called north, east and earth geographic coordinate. The related quantities are marked with right subscript g.

(2) Local vertical local horizontal (LVLH): the origin is located in the satellite center of mass, x axis points to the satellite flight direction; y axis points to the negative direction of normal direction of orbital plane; z axis is defined as per right hand rule, it points to the earth center when the orbit is circular. The orbit system is an important reference system for attitude control. The related quantities are marked with right superscript or right subscript O.

(3) Body coordination: the origin is located in the satellite center of mass. Three coordinate axes coincide with the principal axis of inertia of satellite body. The satellite body system and the orbit system point to the same direction when the three-axis attitude of satellite is stable. The fixing and output of most attitude measurers are in relation to the satellite body system. The quantities related to the satellite body system are marked with right superscript or right subscript b.

(4) Earth center inertial coordinate (ECI): the origin is located in the earth center of mass, x axis points to the vernal equinox; z axis points to the north pole along the earth's spin axis; y axis is defined by right hand rule. The orbital motion of satellite in inertial space and the orbital motion of the sun are described in the coordinate system. The related quantities are marked with right superscript or right subscript i.

(5) Earth center earth fixed coordinate (ECEF): the origin is located in the earth center; x axis points to Greenwich zero meridian in the equatorial plane; z axis points to the north pole along the earth's spin axis; y axis is defined by right hand rule. The coordinate system is fixed to the earth. The atmospheric motion and geomagnetic environment in the near-earth space are described in the coordinate system. The related quantities are marked with right superscript or right subscript e.

For the circumterrestrial motion of satellite, the ECI system is used as the basis of motion, and the orbit system is used as the reference coordinate system to describe the satellite with three axes pointing to the earth stably. The coordinate systems are switched as required. The orbit parameters are used; for example, the magnetic field and sun vector in the geomagnetic field and sun vector models in this paper are switched to the orbit system.

2.2. Quaternion attitude description

The quaternion described satellite attitude consists of one scalar part and three vector parts, defined as

$$\boldsymbol{q} = q_0 + q_1 i + q_2 j + q_3 k = \begin{bmatrix} q_0 & q^T \end{bmatrix} \tag{1}$$

where q_0 is the quaternion scalar part, q is the vector part, the four parameters meet the following constraint condition:

$$\sum_{i=0}^{3} q_i^2 = 1 \tag{2}$$

Therefore, only three of the four variables of quaternion are independent. According to Euler's rotation and quaternion definition, the attitude between orbit system and satellite body system is described by quaternion. The attitude rotation matrix corresponding to orbit system to satellite body system is

$$C_o^b = \begin{bmatrix} 1-2\left(q_2^2+q_3^2\right) & 2\left(q_1q_2+q_0q_3\right) & 2\left(q_1q_3-q_0q_2\right) \\ 2\left(q_1q_2-q_0q_3\right) & 1-2\left(q_1^2+q_3^2\right) & 2\left(q_2q_3+q_0q_1\right) \\ 2\left(q_1q_3+q_0q_2\right) & 2\left(q_2q_3-q_0q_1\right) & 1-2\left(q_1^2+q_2^2\right) \end{bmatrix} \tag{3}$$

Note: the quaternion attitude matrix consists of quadratic term of quaternion $\boldsymbol{q}$, so the quaternion $-\boldsymbol{q}=\begin{bmatrix}-q_0 & -q^T\end{bmatrix}^T$ can obtain the attitude matrix shown in Eq. (3). The nonuniqueness of quaternion is consistent with the nonuniqueness of Euler axis/angle. For example, if the Euler rotation angle is 0 and 2π respectively, the corresponding quaternion is $\begin{bmatrix}1 & 0 & 0 & 0\end{bmatrix}^T$ and $\begin{bmatrix}-1 & 0 & 0 & 0\end{bmatrix}^T$ respectively, but they represent the same attitude and the same rotation actually in physical significance. This paper uses positive value of quaternion for calculation, Eq. (3) is written in vector form, then

$$C_o^b = I_3 - q_0\mathrm{q}^{\times} + \left(\mathrm{q}^{\times}\right)^2 \tag{4}$$

or

$$C_o^b = \left(q_0^2 - \mathrm{q}^T\mathrm{q}\right)I_3 + 2\mathrm{q}\mathrm{q}^T - 2q_0\mathrm{q}^{\times} \tag{5}$$

where $\mathrm{q}^{\times}$ represents the skew symmetric matrix

$$\mathrm{q}^{\times} = \begin{bmatrix} 0 & -q_3 & q_2 \\ q_3 & 0 & -q_1 \\ -q_2 & q_1 & 0 \end{bmatrix} \tag{6}$$

2.3. *Properties of attitude rotation matrix*

The attitude rotation matrix C_o^b described by Eq. (3) can be expressed as

$$C_o^b = \begin{bmatrix}\boldsymbol{c}_1 & \boldsymbol{c}_2 & \boldsymbol{c}_3\end{bmatrix} \tag{7}$$

where $\boldsymbol{c}_i = \begin{bmatrix}c_{1i} & c_{2i} & c_{3i}\end{bmatrix}^T$, $i=1,2,3$ represents the direct cosine vector. C_o^b is the orthogonal matrix, the properties are described below

$$C_o^b = \left(C_b^o\right)^{-1} = \left(C_b^o\right)^T,\ \boldsymbol{c}_1\times\boldsymbol{c}_2 = \boldsymbol{c}_3,\ \boldsymbol{c}_2\times\boldsymbol{c}_3 = \boldsymbol{c}_1,\ \boldsymbol{c}_3\times\boldsymbol{c}_1 = \boldsymbol{c}_2,\ \left(c_{1i}\right)^2 + \left(c_{2i}\right)^2 + \left(c_{3i}\right)^2 = 1,\ and\ \left(c_{j1}\right)^2 + \left(c_{j2}\right)^2 + \left(c_{j3}\right)^2 = 1 \tag{8}$$

The projection of angular rate of satellite body system in relation to orbit system in the satellite body system is defined as ω_o^b, the following relationship can be deduced for the attitude rotation matrix C_o^b

$$\dot{C}_o^b = -C_o^b\left(\omega_o^b\right)^{\times},\ \dot{\boldsymbol{c}}_i = \boldsymbol{c}_i\times\omega_o^b = \left(\boldsymbol{c}_i\right)^{\times}\omega_o^b \tag{9}$$

3. Micro-Satellite Attitude Control Model

3.1. *Micro-satellite thrust-torque deduction*

In Fig. 1 (a) and (b) show the discoid and asymmetrical micro-satellite, the four thrust nozzles of the micro-satellite are in the *x*-*z* plane at inclination α, the nozzles point to y-direction, laid in square at intervals of *d*. The fuel tank is at the *x*-*z* plane l of the nozzle, and is at -*y* distance from the centroid position of the micro-satellite. The Formosat-3 micro-satellite body coordinates are shown in Fig.1 (c), $\Delta\alpha$, Δd and Δl represent the uncertainty of nozzle inclination, relative distance between nozzles and the fuel tank centroid position offset respectively. The nozzle thrust direction and the force arm generated torqueses are deduced as follows:

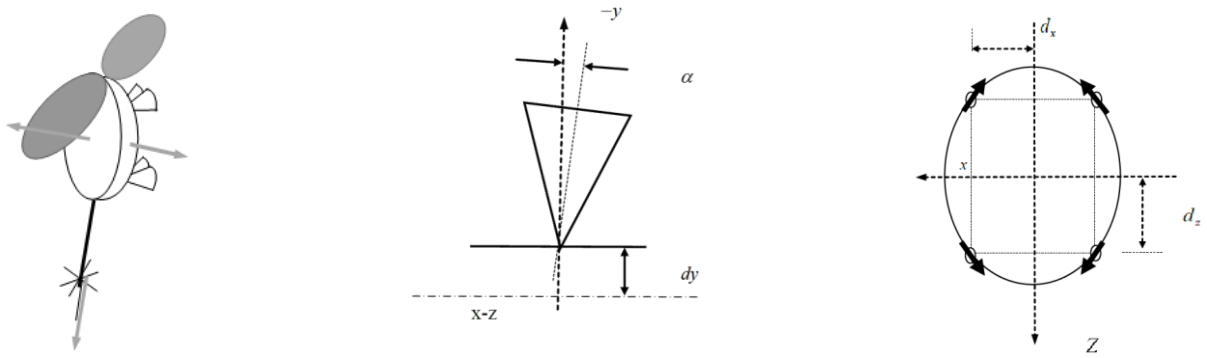

(a) (b) (c)

Fig. 1 (a) Geometric graph of micro-satellite; (b) Thruster geometric arrangement; (c) Thruster geometric arrangement array

$$\begin{aligned}
\vec{F}_1 &= -\frac{1}{\sqrt{2}}\sin(\alpha+\Delta\alpha)\vec{e}_x + \cos(\alpha+\Delta\alpha)\vec{e}_y + \frac{1}{\sqrt{2}}\sin(\alpha+\Delta\alpha)\vec{e}_z \\
\vec{F}_2 &= \frac{1}{\sqrt{2}}\sin(\alpha+\Delta\alpha)\vec{e}_x + \cos(\alpha+\Delta\alpha)\vec{e}_y + \frac{1}{\sqrt{2}}\sin(\alpha+\Delta\alpha)\vec{e}_z \\
\vec{F}_3 &= \frac{1}{\sqrt{2}}\sin(\alpha+\Delta\alpha)\vec{e}_x + \cos(\alpha+\Delta\alpha)\vec{e}_y - \frac{1}{\sqrt{2}}\sin(\alpha+\Delta\alpha)\vec{e}_z \\
\vec{F}_4 &= -\frac{1}{\sqrt{2}}\sin(\alpha+\Delta\alpha)\vec{e}_x + \cos(\alpha+\Delta\alpha)\vec{e}_y - \frac{1}{\sqrt{2}}\sin(\alpha+\Delta\alpha)\vec{e}_z
\end{aligned} \tag{10}$$

$$\begin{aligned}
\vec{r}_1 &= (d_x+\Delta d_x)\vec{e}_x - (l+\Delta l)\vec{e}_y + (d_y+\Delta d_y)\vec{e}_z \\
\vec{r}_2 &= -(d_x+\Delta d_x)\vec{e}_x - (l+\Delta l)\vec{e}_y + (d_z+\Delta d_z)\vec{e}_z \\
\vec{r}_3 &= -(d_x+\Delta d_x)\vec{e}_x - (l+\Delta l)\vec{e}_y - (d_z+\Delta d_z)\vec{e}_z \\
\vec{r}_4 &= (d_x+\Delta d_x)\vec{e}_x - (l+\Delta l)\vec{e}_y - (d_z+\Delta d_z)\vec{e}_z
\end{aligned} \tag{11}$$

where

$$\left|\frac{\Delta d_x}{d_x}\right| \le 0.2,\ \left|\frac{\Delta d_z}{d_z}\right| \le 0.2,\ \left|\frac{\Delta l}{l}\right| \le 0.2, \text{ and } \left|\frac{\Delta\alpha}{\alpha}\right| \le 0.2. \tag{12}$$

If $\alpha+\Delta\alpha$ is very small, the torque τ_u can be deduced as follows:

$$\begin{bmatrix} \tau_{u_x} \\ \tau_{u_y} \\ \tau_{u_z} \end{bmatrix} = \begin{bmatrix} \vec{r}_1\times\vec{F}_1 & \vec{r}_2\times\vec{F}_2 & \vec{r}_3\times\vec{F}_3 & \vec{r}_4\times\vec{F}_4 \end{bmatrix} \begin{bmatrix} u_1 \\ u_2 \\ u_3 \\ u_4 \end{bmatrix}$$

$$= \begin{bmatrix} -\beta_{1\Delta} & -\beta_{1\Delta} & \beta_{1\Delta} & \beta_{1\Delta} \\ -\beta_{2\Delta} & \beta_{2\Delta} & -\beta_{2\Delta} & -\beta_{2\Delta} \\ \beta_{3\Delta} & -\beta_{3\Delta} & -\beta_{3\Delta} & \beta_{3\Delta} \end{bmatrix} \begin{bmatrix} u_1 \\ u_2 \\ u_3 \\ u_4 \end{bmatrix}, \tag{13}$$

$$= \boldsymbol{\beta} u$$

where $\beta_{i\Delta} = \beta_i + \Delta\beta_i,\ i = 1,2,3$

$$\beta_1 = d + \frac{\alpha l}{\sqrt{2}}, \quad \beta_2 = \sqrt{2}\alpha d, \quad \beta_3 = d - \frac{\alpha l}{\sqrt{2}}$$

$$\Delta\beta_1 = \Delta d + \frac{1}{\sqrt{2}}\left(\alpha\Delta l + l\Delta\alpha + \Delta\alpha\Delta l\right), \tag{14}$$

$$\Delta\beta_2 = \sqrt{2}\left(\alpha\Delta l + l\Delta\alpha + \Delta\alpha\Delta l\right),$$

$$\Delta\beta_3 = \Delta d - \frac{1}{\sqrt{2}}\left(\alpha\Delta l + l\Delta\alpha + \Delta\alpha\Delta l\right)$$

3.2. *On/off-modulated thrust control*

The procedure to convert the controller to pulse-width modulation is:

(1) The thruster commands: $\boldsymbol{u}$.

(2) Convert $\boldsymbol{u}$ (n) from variable thrusts for the fixed total sample period to fixed thrusts for variable times: *t*_on = (sample time/thrust magnitude)× $\boldsymbol{u}$.

(3) Limit on-times to ± half the sample period.

(4) Compute a bias term, add the bias to all on-times such that at least one thruster is on for the complete sample period.

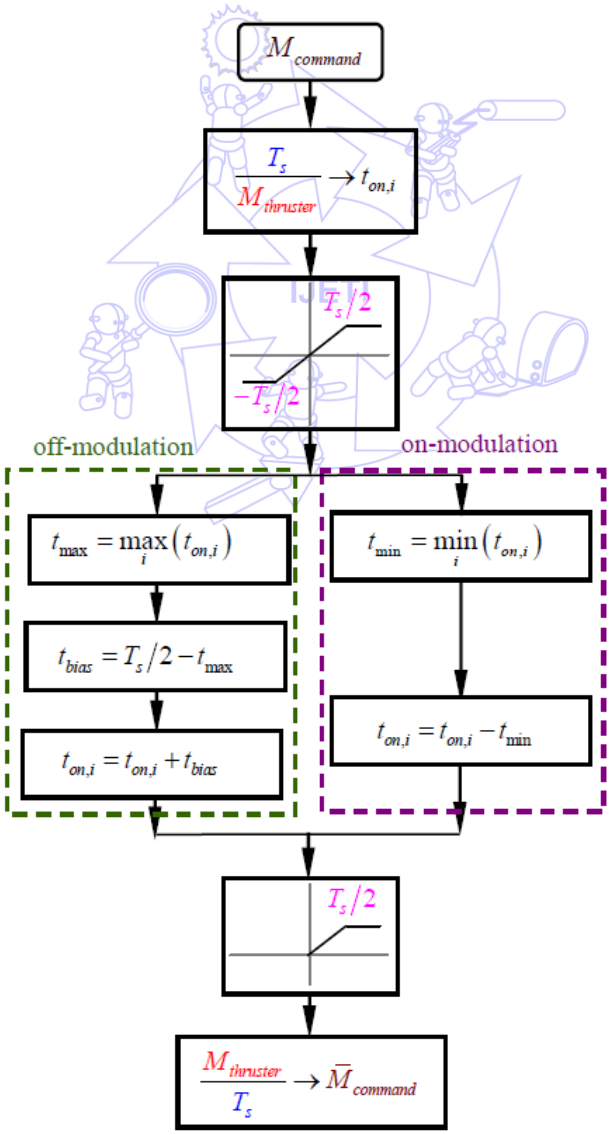

Fig. 2 Block diagram of on/off-modulated thrust control

According to the PWM duty rule, the duty period can be divided into two modulations: off-modulation and on-modulation. Off-modulation mode, in the entire operating cycle has at least one thrust operates; work in on-modulation mode, work the entire period, with at least one thrust control does not work. In this project, an on-modulation is adopted. Micro-satellite attitude control Pulse-width modulation block diagram shown in Fig. 2 which shows PWM processing, from the control flow chart of Pulse-width on/off Modulation algorithm, there is at least one thruster works in the off-modulation, while there is at least one thruster does not work in the on-modulation. In Fig. 2, $M_{thruster}$ and T_s represents the maximum amplitude of the thruster, sampling time.

4. Unscented Kalman Filter

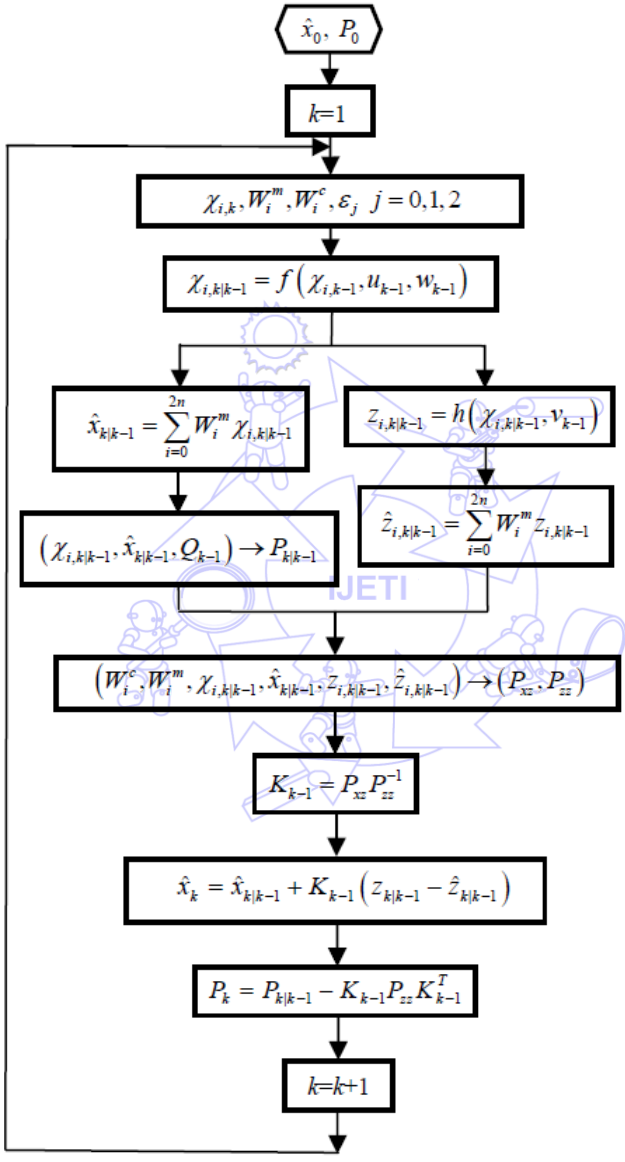

Fig. 3 Flow chart of unscented kalman filter algorithm

In the course of satellite attitude determination filter, in order to solve the nonlinear problem of state equation and measure equation, the normal method is to use extended kalman filter (EKF) for linear approximation of nonlinear function, and the higher-order terms of approximate expansion are neglected in the course of approximation. The EKF process results in the following problems: when the higher-order terms of Taylor expansion of nonlinear function cannot be neglected, the linearization results in major errors in the system, even makes the filter difficult to be stable in the iterative process. It is difficult to find out Jacobian matrix derivation of nonlinear function in many problems. In order to increase the accuracy of

filter and to improve the performance of filter, this paper uses unscented kalman filter (UKF) algorithm in the satellite attitude determination process [3, 4].

The state equation and measure equation of UKF have the following standard forms,

$$\boldsymbol{x}_{k+1} = f\left(\boldsymbol{x}_k, \boldsymbol{u}_k, \boldsymbol{w}_k\right) \tag{15}$$

$$\boldsymbol{x}_{k+1} = f\left(\boldsymbol{x}_k, \boldsymbol{u}_k, \boldsymbol{w}_k\right) \tag{16}$$

where $\boldsymbol{x}_k$ is the n-dimensional state vector of the system, and the variance is set as P_k; $\boldsymbol{u}_k$, is *r*-dimensional input vector; f is n-dimensional vector function; *h* is *m*-dimensional vector function; $\boldsymbol{w}_k$ is *p*-dimensional stochastic process noise, the variance matrix is Q; $\boldsymbol{v}_k$ is *q*-dimensional random noise, the variance matrix is R.

The difference between UKF and EKF is that the UKF uses sampling point conversion to calculate the state and measure the average value and variance of forecast values. The sampling point conversion process is that the average value and variance of estimates generate a group of discrete sampling points, these points are spread by state equation and measure equation, and then the average value and variance of the forecast values are generated by weighted summation. The generation of sampling points is shown below:

The augmented state variable is $\hat{\boldsymbol{x}} = \left[\boldsymbol{x}_k^T, \boldsymbol{w}_k^T, \boldsymbol{v}_k^T\right]^T$

(1) Select ε sampling points

$$\chi_{0,k} = \hat{x}_k \tag{17a}$$

$$\chi_{i,k} = \hat{x}_k + \left(\sqrt{(n+\varepsilon_0)P_k}\right)_i^T, \quad i = 1, 2, \cdots, n \tag{17b}$$

$$\chi_{i+n,k} = \hat{x}_k - \left(\sqrt{(n+\varepsilon_0)P_k}\right)_i^T, \quad i = 1, 2, \cdots, n \tag{17c}$$

(2) Calculate weights:

$$W_0^m = \frac{\varepsilon_0}{(n+\varepsilon_0)} \tag{18a}$$

$$W_0^c = W_0^m + \left(1 - \varepsilon_1^2 + \varepsilon_2\right) \tag{18b}$$

$$W_i^m = W_i^c = \frac{1}{2(n+\varepsilon_0)}, \quad i = 1, 2, \cdots, n \tag{18c}$$

where $\varepsilon_0 = \varepsilon_1^2(n+\kappa) - n$, ε_1 and κ are undetermined parameters, ε_1 is set as a small positive number $\left(e.g., 10^{-4} \le \varepsilon_1 \le 1\right)$, it determines the range of sampling points circling $\hat{x}$, the influence of higher-order terms of nonlinear equation can be reduced by regulating ε_1. The accuracy of variance can be increased by regulating ε_2. The optimal ε_2 is 2 in Gaussian distribution. κ is a scale factor which is 2 when the system is univariable, let $\kappa = 3 - n$ if it is multivariable. $\left(\sqrt{(n+\varepsilon_0)P_k}\right)_i$ represents No. i row of matrix root.

5. Measurement Reference Model

5.1. Geomagnetic field model

The International Geomagnetic Reference Field (IGRF) model [2] is used in this paper as the mathematical simulation model of geomagnetic field of gyroless satellite, r in Eq. (19) is the distance between the satellite and the earth center in ECEF, λ is the longitude of the satellite in the ECEF, ϑ is the colatitude of satellite in the ECEF (90^o minus latitude), $R_\oplus$ is the major semi-axis of the earth (6371.2 km), g and h are the Gaussian coefficients of IGRF model, P_n^m is Legendre function, $m \le n$. Since the Gaussian coefficients g_n^m and h_n^m used in IGRF model are derived from the measured geomagnetic field by least square matching, the Gaussian coefficients should be remeasured and updated about every five years [1]. The order number of Gaussian coefficients of IGRF model is 10, so n in Eq. (19) can be 1 to ∞, and m is 0 to n.

$$V(r,\lambda,\vartheta) = R_\oplus \bullet \sum_{n=1}^{\infty}\sum_{m=0}^{n}\left(\frac{R_\oplus}{r}\right)^{n+1}\left(g_n^m \cos(m\lambda) + h_n^m \sin(m\lambda)\right)P_n^m(\vartheta) \tag{19}$$

The geomagnetic field vector $\boldsymbol{B}_g$ can be derived from the negative gradient of geomagnetic field potential function V in Eq. (20)

$$\boldsymbol{B}_g = -\nabla V \tag{20}$$

The relational expression of geomagnetic field vector $\boldsymbol{B}_g$ and satellite position, i.e. the component of magnetic field V in the north, east and earth directions in the geographic coordinate system. The relationship between the geomagnetic field vector and the satellite position can be obtained

$$\begin{aligned}\boldsymbol{B}_g &= \begin{bmatrix} B_x & B_y & B_z \end{bmatrix}^T \\ &= \begin{bmatrix} \frac{1}{r}\frac{\partial V}{\partial \vartheta} & -\frac{1}{r\sin\vartheta}\frac{\partial V}{\partial \lambda} & \frac{\partial V}{\partial r} \end{bmatrix}^T\end{aligned} \tag{21}$$

The IGRF described geomagnetic field intensity is calculated by the ECEF, the relation of geomagnetic field vector $\boldsymbol{B}_g$ in the spherical coordinates of geomagnetic field and the earth centered inertial coordinate system *i* shows as long as the north, east and earth geomagnetic coordinates circle around oY_λ axis by $(180-\vartheta)$ in turn, and circle around oX_ϑ by $-\alpha$, the earth centered inertial coordinate system is obtained. The transition matrix C_g^i of geographic coordinate system to earth centered inertial coordinate is

$$C_g^i = C_x(-\alpha)C_y(180-\vartheta),\ \boldsymbol{B}_i = C_g^i \boldsymbol{B}_g \tag{22}$$

In Eq. (22), $\alpha = (\lambda + G)$ is the right ascension, G is the Greenwich right ascension of meridian or GST.

For simulation analysis, the IGRF model is used to simulate the real geomagnetic field. The tenth-order spherical order number is selected for simulation, ensuring high enough geomagnetic field accuracy. Certainly, for the geomagnetic field model loaded on real satellite, as the operational performance of the satellite carried calculator is limited, the magnetic field model series cannot be too high. It is determined according to the performance of magnetometer and the attitude determination accuracy by simulation. For the orbit at altitude of 500km and inclination of 72^o, the magnetic field intensity of tenth-order IGRF in the orbit system is shown in Fig. 4.

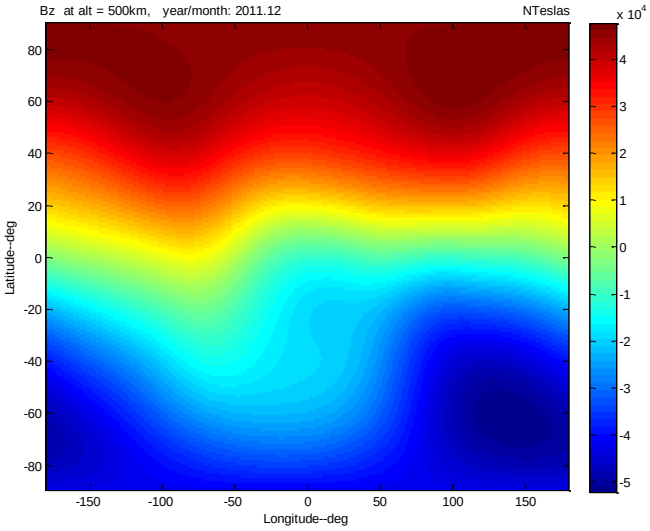

Fig. 4 Magnetic field distribution of micro-satellite in orbital coordinates

5.2. *Magnetometer model*

The magnetometer uses geomagnetic field as the basis of attitude measurement. The three magnetometers are fixed along three axes of body coordination to measure local magnetic field intensity of three axes. The three-axis attitude of the satellite can be estimated by comparing it with the magnetic field model of given environment. The three-axis magnetometer is fixed along the satellite body axis to measure the body yaw angle. Assume $\boldsymbol{B}_g = \begin{bmatrix} B_x & B_y & B_z \end{bmatrix}^T$ to be the component of geographic coordinate of geomagnetic field, and assume C_g^i and C_i^o to be the transition matrix of geographic coordinate system into earth centered inertial coordinate system and the transition matrix of earth centered inertial coordinate system into orbital coordinate system. The component of geomagnetic field vector in the orbit system can be expressed as:

$$\boldsymbol{B}_o = C_i^o C_g^i \boldsymbol{B}_g \tag{23}$$

The component of geomagnetic field in the satellite body system can be derived from the measured value and estimated value respectively:

$$\boldsymbol{B}_b = C_o^b C_i^o C_g^i \boldsymbol{B}_g + \upsilon_b \tag{24}$$

where υ_b is a zero mean white noise, i.e.

$$\upsilon_b \sim \left(0, \sigma_g^2\right) \tag{25}$$

5.3. *Sun vector model*

The satellite attitude is estimated by the vector observation obtained by sun sensor. It is required to know the sun vector in the orbit system, and can be determined according to the solar ephemeris and orbit parameters. This paper uses the method of literature [2], building the sun model based on the relationship between the earth and the sun. Since the included angle between the sunray and the equatorial plane of the earth changes periodically within tropics of Capricorn and Cancer $\pm 23^\circ$ during a year, the sunray elevation in the earth centered inertial system is

$$\varepsilon_s = \frac{23\pi}{180} \sin\left(\frac{2\pi T_\Psi}{365}\right) \tag{26}$$

where T_Ψ is the time counted since the vernal equinox. The sun azimuth starting from vernal equinox within one year is

$$\lambda_s = \frac{2\pi T_\Psi}{365} \tag{27}$$

When the earth passes by the vernal equinox, the unit vector of sunray position in the earth centered inertial system is $s_0^{\varpi_i} = [1 \quad 0 \quad 0]^T$, then the sun vector at any time is

$$s^{\varpi_i} = C_y(\varepsilon_s)C_z(\lambda_s)s_0^{\varpi_i},\ s^{\varpi_o} = C_i^o s^{\varpi_i},\ C_i^o = C_z(\omega+v)C_x(i)C_z(\Omega) \tag{28}$$

where s^{ϖ_i} is the sun vector in the ECI, s^{ϖ_o} is the sun vector in the orbit system, C_i^o is the transition matrix of ECI into orbit system. According to the model, the sun vectors in the inertial system and orbit system within one year from the vernal equinox are shown in Fig. 5.

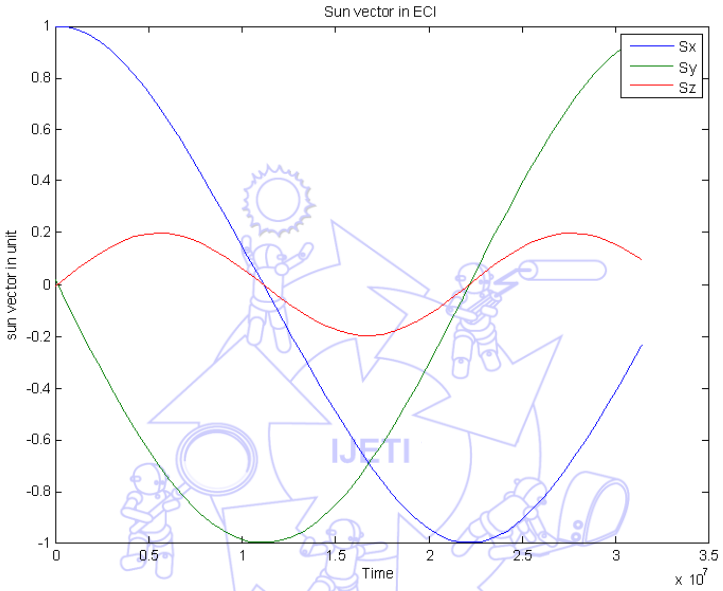

Fig. 5 Sun vector in inertial system within one year from vernal equinox

5.4. *CSS reading algorithm*

(1) CSS geometric configuration and sun vector:

If the micro-satellite uses eight CSS's to calculate the sun vector, based on the present orientation configuration and FOV values of CSS, there will be at most four CSS's irradiated by the sun, and then three and two in sun illumination. Thus, the algorithm varies with three different cases.

Let the real sun vector be:

$$\boldsymbol{S}_{real} = \left[S_{real\_x} \quad S_{real\_y} \quad S_{real\_z}\right]^T \tag{29}$$

The relationship between the current generated by eight CSS's and the sun vector is

$$\boldsymbol{I}_i = \boldsymbol{I}_0 \boldsymbol{N} \boldsymbol{S}_{real} \tag{30}$$

where $\boldsymbol{I}_i = [I_1 \quad I_2 \quad \cdots \quad I_8]^T$ is the current generated by various CSS's in sun illumination; $\boldsymbol{I}_0$ is the maximum current output of CSS (for Formosat-3 $\boldsymbol{I}_0 = 167mA$); $\boldsymbol{N}$ is the normal vector orientation of eight CSS's.

$$\boldsymbol{N} = \begin{bmatrix} N_1 \\ N_2 \\ N_3 \\ N_4 \\ N_5 \\ N_6 \\ N_7 \\ N_8 \end{bmatrix} = \begin{bmatrix} a_1 & b_1 & c_1 \\ a_2 & b_2 & c_2 \\ a_3 & b_3 & c_3 \\ a_4 & b_4 & c_4 \\ a_5 & b_5 & c_5 \\ a_6 & b_6 & c_6 \\ a_7 & b_7 & c_7 \\ a_8 & b_8 & c_8 \end{bmatrix} \tag{31}$$

(2) Cases of four, three and two CSS's in sun illumination:

There are 2,000 data samples for regime analysis of 5% reading error of CSS (in relation to reading) and 70° FOV of CSS respectively, as shown in Fig. 6. (Note: read noise of sensor is noise of normal Gaussian distribution)

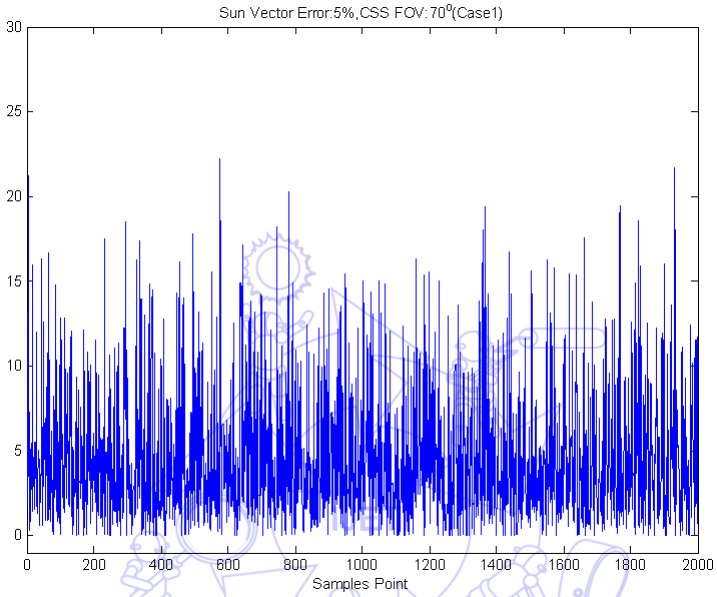

Fig. 6 Sensor reading error 5%, CSS FOV: 70°

5.5. Earth horizon sensor model

The infrared earth sensor is known as infrared horizon sensor. It is an important assembly of different kinds of satellite attitude control systems, and its performance and working stability influence the overall safety of satellite directly. As an attitude measurement component, it is extensively used in satellite design, from low orbit earth resources observation satellite to high orbit synchronous communication satellite. All of these use it as measurement component for pitch and roll attitude angles of satellite. The static infrared horizon sensor is also known as radiant heat balance earth sensor. The static horizon sensor is fixed to the side toward the earth of the satellite, composed of 14-16μm filter lenses and four thermopile detectors. Its principal optic axis is parallel to the Oz-axis of satellite, as shown in Figure 7. The included angles between the spectral axes of four detectors and the principal optic axis can be obtained according to the distance of the satellite to the earth, so as to keep the FOV of four detectors in the center of the earth disc, as shown in Figure 8. When the satellite attitude has a deviation, the output of four probes will change accordingly, then

$$\varphi = \frac{\delta_2 - \delta_4}{2} \tag{31}$$

$$\theta = \frac{\delta_1 - \delta_3}{2} \tag{32}$$

where φ is the roll attitude angle of satellite, θ is the pitch attitude angle.

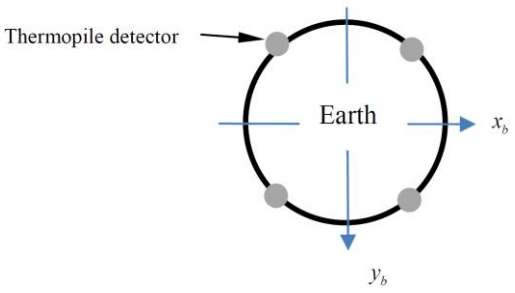

Fig. 7 Schematic of static horizon sensor sweeping earth

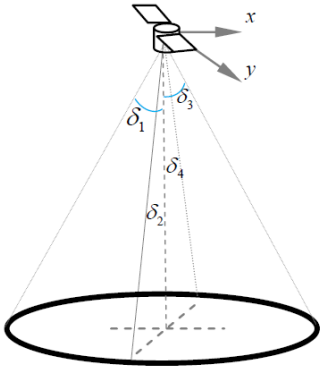

Fig. 8 Attitude measuring of static horizon sensor

6. Nonlinear H_∞ Robust Control Law

The micro-satellite kinematic equation is described by

$$\dot{\underline{q}} = \frac{1}{2}\begin{bmatrix} -\underline{\omega}^{\times} & \underline{\omega} \\ -\underline{\omega}^{T} & 0 \end{bmatrix}\begin{bmatrix} \mathbf{q} \\ q_4 \end{bmatrix} = \frac{1}{2}\begin{bmatrix} \mathbf{q}^{\times} + q_4 I \\ -\mathbf{q}^{T} \end{bmatrix}\underline{\omega} = \frac{1}{2}Q(\underline{q})\underline{\omega} \tag{33}$$

where

$$Q(\underline{q}) \triangleq \frac{1}{2}\begin{bmatrix} \mathbf{q}^{\times} + q_4 I \\ -\mathbf{q}^{T} \end{bmatrix} \tag{34}$$

In the attitude control design, it is desired that the system is stable and the excursions of the angular rate and control input are minimized. This motivates the use of the following penalty function to be minimized

$$\underline{z} = \begin{bmatrix} \sqrt{\rho_1 \underline{\omega}^T J_\Delta \underline{\omega} + \rho_2 \eta^2(q_4)} \\ \rho_3 \underline{u} \end{bmatrix} \tag{35}$$

where ρ_1, ρ_2 and ρ_3 are weighting coefficients introduced for the trade-off between performance and control effort. The function $\eta(q_4)$ is defined as $\eta(q_4) = 2\cos^{-1}|q_4|$.

The attitude control problem can then be formulation as

$$\dot{\underline{x}} = \left(f(\underline{x}) + \Delta f(\underline{x})\right) + \left(g_1(\underline{x}) + \Delta g_1(\underline{x})\right)\underline{w} + \left(g_2(\underline{x}) + \Delta g_2(\underline{x})\right)\underline{u} \tag{36}$$

$$\underline{z} = \begin{bmatrix} h(\underline{x}) \\ \underline{u} \end{bmatrix} = h_1(\underline{x}) \tag{37}$$

where $\underline{x} = \begin{bmatrix} \underline{\omega}^T & \underline{\mathrm{q}}^T & q_4 \end{bmatrix}^T$ is the state $\underline{x}$ and $\underline{w}$ is the disturbance. The Δf, $\Delta \mathrm{g}_1$ and $\Delta \mathrm{g}_2$ are uncertain smooth vector fields and mappings. Denote $\delta J = J^{-1}\Delta J J^{-1}$, for small perturbations, f, g_1, g_2, h_1, Δf, $\Delta \mathrm{g}_1$ and $\Delta \mathrm{g}_2$ can be expressed as

$$f(\underline{x})=\begin{bmatrix} -J^{-1}\underline{x}_1^{\times}J\underline{x}_1 \\ Q(\underline{x}_2)\underline{x}_1 \end{bmatrix},\ g_1(\underline{x})=\begin{bmatrix} J^{-1} \\ 0 \end{bmatrix}, g_2(\underline{x})=\begin{bmatrix} J^{-1}B \\ 0 \end{bmatrix},$$

$$h_1(x)=\sqrt{\rho_1\underline{x}_1^{T}J\underline{x}_1+\rho_2\eta^2(q_4)}, \tag{38}$$

$$\Delta f(\underline{x})=\begin{bmatrix} -J^{-1}\underline{x}_1^{\times}J\underline{x}_1+J^{-1}\delta J\underline{x}_1^{\times}J\underline{x}_1+J^{-1}\delta J\underline{x}_1^{\times}\Delta J\underline{x}_1 \\ 0 \end{bmatrix},$$

$$\Delta g_1(\underline{x})=\begin{bmatrix} -\delta J \\ 0 \end{bmatrix},\ \Delta g_2(\underline{x})=\begin{bmatrix} J^{-1}\Delta B-\delta J(B+\Delta B) \\ 0 \end{bmatrix}, \text{ etc.}$$

6.1. *Nonlinear H_∞ robust control theory*

Consider a nonlinear state-space system G_0

$$\dot{\underline{x}}=f(\underline{x})+g(\underline{x})\underline{w} \tag{39a}$$

$$\underline{z}=h(\underline{x}) \tag{39b}$$

where $\underline{x}$ is the state vector, $\underline{w}$ is the exogenous disturbance to be rejected, and $\underline{z}$ is the penalized output signal. We assume that $f(\underline{x})$, $g(\underline{x})$, and $h(\underline{x})$ are C^∞ functions and $\underline{x}=0$ is the equilibrium point of the system, that is, $f(0)=h(0)=0$.

Given a positive number $\gamma>0$, system (3) has a finite L_2-gain less than γ if for all $\underline{w}\in L_2[0,T]$ with $0\le T<\infty$,

$$\int_0^T\|\underline{z}(t)\|^2\,dt\le\gamma^2\int_0^T\|\underline{w}(t)\|^2\,dt \tag{40}$$

Lemma 1 Assume that $\Delta f(\underline{x})=0$, $\Delta g_1(\underline{x})=0$ and $\Delta g_2(\underline{x})=0$ in Eq.(33). If $(f(\underline{x}),h_1(\underline{x}))$ is zero-detectable and there exists a positive-definite function $V(\underline{x})$ such that the following Hamilton-Jacobi partial differential inequality holds [4]:

$$H_\gamma=V_{\underline{x}}^{T}f+\frac{1}{2}V_{\underline{x}}^{T}\left(\frac{1}{\gamma^2}g_1g_1^{T}-g_2g_2^{T}\right)V_{\underline{x}}+\frac{1}{2}h_1^{T}h_1<0 \tag{41}$$

Then the system has a finite L_2 gain less than γ. Once $V(\underline{x})$ is found, the control signal $\underline{u}$ can be synthesized as

$$\underline{u}=-g_2^{T}V_{\underline{x}} \tag{42}$$

where

$$V_{\underline{x}}=\left[\frac{\partial V}{\partial x_1}\quad\frac{\partial V}{\partial x_2}\quad\cdots\quad\frac{\partial V}{\partial x_n}\right]^{T}. \tag{43}$$

Theorem 1 Consider the nonlinear uncertain system (33) and the uncertainty of system parameters satisfies the following Eq. (44) [5].

$$\Delta f(\underline{x})=\Phi(\underline{x})\Psi^{T}(\underline{x}),\ \Delta g_1(\underline{x})\Delta g_1^{T}(\underline{x})\le G_1(\underline{x})G_1^{T}(\underline{x}),\ \textit{and}\ \Delta g_2(\underline{x})\Delta g_2^{T}(\underline{x})\le G_2(\underline{x})G_2^{T}(\underline{x}), \tag{44}$$

where $\Phi(\underline{x}) \in \square^{n\times m}$, $\Psi(\underline{x}) \in \square^{1\times m}$ and $G_i(\underline{x}) \in \square^{n\times p_i}$, $i=1,2$ are known vector, for which we assume that there exist scale functions $\Theta(\underline{x}) \geq 0$ with $\Psi(\underline{x})$ described by $\|\Psi(\underline{x})\| \leq \Theta(\underline{x})$ with $\Theta(0)=0$. Under this assumption, if system (3) satisfies the following conditions:

(i) $\left(f(\underline{x})+\Delta f(\underline{x}), h_1(\underline{x})\right)$ is zero-state detectable.

(ii) There exists a smooth function $\sigma=\sigma(\underline{x})>0$ such that the following Hamilton -Jacobi partial differential inequality

$$V_{\underline{x}}^T f+\frac{1}{2}V_{\underline{x}}^T\left(\frac{1}{\gamma^2}(1+\sigma)g_1g_1^T-(1-\sigma)g_2g_2^T\right)V_{\underline{x}}+\frac{1}{2}V_{\underline{x}}^T\left(\frac{1}{\gamma^2}\frac{1+\sigma}{\sigma}G_1G_1^T+\frac{1-\sigma}{\sigma}G_2G_2^T+\sigma\Phi\Phi^T\right)V_{\underline{x}}+\frac{1}{2\sigma}\Psi^T\Psi+\frac{1}{2}h_1^Th_1\leq 0 \tag{45}$$

has a smooth positive solution $V(\underline{x})$ where $\underline{x}\in X$, and X is an neighborhood of origin in $\square^n$, then by the following state feedback law:

$$u(\underline{x})=-g_2^TV_{\underline{x}} \tag{46}$$

the closed-loop system of (33) has a robust H_∞-performance.

7. Attitude Determination Subsystem Analysis

7.1. CSS + scanning horizon sensor + three-axis magnetometer satellite attitude estimation

(1) Attitude estimation state variable:

The nine-dimensional attitude estimation state variable is used for micro-satellite

$$\hat{\boldsymbol{x}}=\left[\hat{\phi}\quad\hat{\theta}\quad\hat{\psi}\quad\dot{\hat{\phi}}\quad\dot{\hat{\theta}}\quad\dot{\hat{\psi}}\quad\int\hat{\phi}\quad\int\hat{\theta}\quad\int\hat{\psi}\right]^T \tag{47}$$

(2) Direct observation equation:

If the attitude is measured only by CSS, horizon sensor and magnetometer instead of gyro, the measurement output of CSS, horizon sensor and magnetometer is adopted directly as the observations. The filter output value should be compared with the observed value, so the most straightforward observation vector can be selected as the measured value of sun vector $\boldsymbol{S}_b$, horizon sensor $\boldsymbol{E}_b$ and three-dimensional geomagnetic field vector $\boldsymbol{B}_b$ in the satellite body system, i.e.

$$z=\left[\boldsymbol{S}_b^T\quad\boldsymbol{E}_b^T\quad\boldsymbol{B}_b^T\right]^T=\left[S_{bx}\quad S_{by}\quad S_{bz}\mid E_{bx}\quad E_{by}\quad E_{bz}\mid B_{bx}\quad B_{by}\quad B_{bz}\right]^T \tag{48}$$

The corresponding measure equation is

$$z=h(\boldsymbol{x})+\boldsymbol{v}=\begin{bmatrix}C_o^b(\boldsymbol{x})\boldsymbol{S}_o\\C_o^b(\boldsymbol{x})\boldsymbol{E}_o\\C_o^b(\boldsymbol{x})\boldsymbol{B}_o\end{bmatrix} \tag{49}$$

where $\boldsymbol{v}=\left[\boldsymbol{v}_S^T\quad\boldsymbol{v}_E^T\quad\boldsymbol{v}_B^T\right]^T$ is the measurement noise of CSS, horizon sensor and magnetometer. $\boldsymbol{S}_o$, $\boldsymbol{E}_o$ and $\boldsymbol{B}_o$ are the sun vector, earth radiation and geomagnetic field vector respectively calculated according to the orbital location look-up table of satellite.

(3) Simulation results and analysis:

The gyroless UKF designed in this section is simulated. As the satellite experiences attitude large-angle motion and attitude stabilization motion in the attitude capture process, the attitude changes frequently. Therefore, the attitude changes in the satellite attitude capture are selected as objects for attitude filter estimation, from the filter effect of CSS + scanning horizon sensor + three-axis magnetometer on gyroless UKF in this section.

(4) Simulated conditions:

The magnetometer measurement error is 500 nT, the solar sensor measurement error is 10%, satellite attitude three-axis initial attitude is different from UKF initial attitude, the Satellite altitude 500 km, longitude 108°, latitude 35°. Sampling time 4sec, On-modulator magnitude = 2, satellite attitude motion trajectory is shown in Figure 9. The CSS tasks decrease from four tasks to two CSS tasks at 200 sec, CSS does not work when the satellite enters the earth's shadow area at 600 sec. The UKF of direct observation equation is used. The simulation results show when the CSS + scanning horizon sensor + three-axis magnetometer work normally, the estimated large-angle attitude change has relatively small error and the maximum error is 10°. If the number of CSS tasks is reduced, the error is relatively large when the attitude changes, the instantaneous maximum error is 32°. The parameters of micro-satellite are shown in following:

$$\begin{bmatrix} d_x & d_y & l & \alpha \end{bmatrix} = \begin{bmatrix} 0.1m & 0.1m & 0.5m & 5\deg \end{bmatrix}, \quad J = \begin{bmatrix} 5.5384 & 0 & 0 \\ 0 & 5.6001 & 0 \\ 0 & 0 & 4.2382 \end{bmatrix} NT \cdot m \tag{49}$$

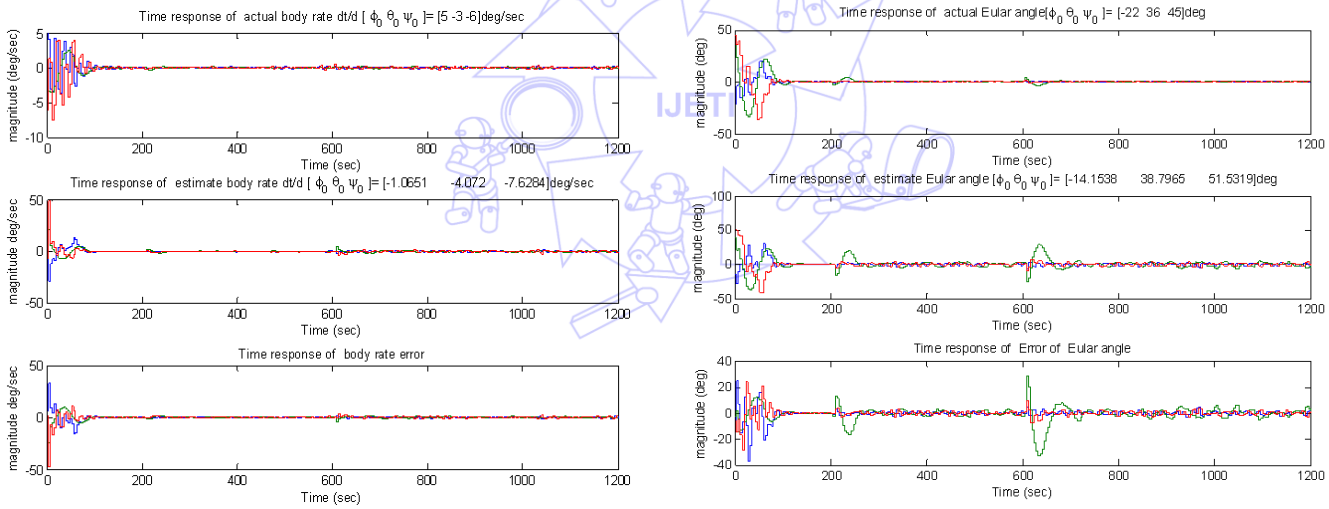

(a) CSS 4→ 2 at 200 sec, CSS 2→ 0 at 600 sec (b) CSS 4→ 2 at 200 sec, CSS 2→ 0 at 600 sec

Fig. 9 Time response of micro-satellite measured and estimated angular rate

Acknowledgements

This study was financially sponsored by the National Science Council under Project No. 101-2221-E-344-002, and the 2012 "Subsidies for Teachers (Instructors) of Military Academies in Academic Research" G.K.R.P.Z. No. 1010005122.

References

[1] P. M. Stoltz, S. Sivapiragasam, and T. Anthony, "Satellite orbit-raising using LQR control with fixed thrusters," Advances in Astronautical Science, pp. 1-13, AAS 98-007, 1998.

[2] J. R. Wertz, "Spacecraft attitude determination and control," Kluwer Academic Publishers, 1978.

[3] H. N. Shou and C. T. Lin, "Micro-satellite detumbling mode attitude determination and control: UKF approach," Storage Management Solutions, no. 5, pp. 35-41, 2011.
[4] H. N. Shou, J. C. Juang, Y. W. Jan, and C. T. Lin, "Quaternion feedback attitude control design: a nonlinear H_∞ approach," Asian Journal of Control, vol. 5, no. 3, pp. 406-411, 2003.
[5] A. Isidori and A. Astolfi, "Disturbance attenuation and H_∞-control via measurement feedback in nonlinear systems," IEEE Transaction on Automatic Control, vol. 37, no. 9, pp. 1283-1293, 1992.